A novel Gappy reduced order method to capture non-parameterized geometrical variation in fluid dynamics problems

Nissrine Akkari, Fabien Casenave, David Ryckelynck

A novel Gappy reduced order method to capture non-parameterized geometrical variation in fluid dynamics problems

Nissrine Akkari*, Fabien Casenave*, David Ryckelynck†
email: nissrine.akkari@safrangroup.com[1]

*Safran Tech, Modelling & Simulation, Rue des Jeunes Bois, Châteaufort, 78114 Magny-Les-Hameaux, France
†Centre des Matériaux, Mines ParisTech PSL Research University, CNRS UMR 7633, 63-65 rue Henri Auguste Desbruères, Corbeil-Essonnes, France

December 2, 2019

Abstract

In this work, we propose a new Gappy reduced order method to fill the gap within an incomplete turbulent and incompressible data field in such a way to satisfy the physical and topological changes of the fluid flow after a non-parameterized geometrical variation in the fluid domain [1]. A single baseline simulation is assumed to be performed prior geometrical variations. The proposed method is an enhancement of the Gappy-POD method proposed by Everson and Sirovich in 1995, in the case where the given set of empirical eigenfunctions is not sufficient and is not interpolant for the recovering of the modal coefficients for each Gappy snapshot by a least squares procedure. This happens when the available data cannot be written as an interpolation of the baseline POD modes. This is typically the

[1]This work extends the one that has been published as a conference proceeding to the 2018 AIAA Scitech Forum and Exposition, see Akkari et al. (2018).

case when we introduce non-parameterized geometrical modifications in the fluid domain. Here, after the baseline simulation, additional solutions of the incompressible Navier-Stokes equations are solely performed over a restricted fluid domain, that contains the geometrical modifications. These local Large Eddy Similations that we will call hybrid simulations are performed by using the immersed boundary technique, where the latter is a fluid boundary and is defined by the baseline velocity field. Then, we propose to repair the POD modes using a local modification of the baseline POD modes in the restricted fluid domain. The modal coefficients of the least squares optimization of the Gappy-POD technique are now well recovered thanks to these updated modes, i.e. the residual of the Gappy-POD technique in the restricted fluid domain is now equal to zero. Furthermore, we will propose a physical correction of the latter enhanced Gappy-POD modal coefficients thanks to a Galerkin projection of the full Navier-Stokes equations upon the new compression modes of the available data. This repairing procedure of the global velocity reconstruction by the physical constraint was tested on a 3D semi-industrial test case of a typical aeronautical injection system. The speed-up relative to this new technique is equal to 100, which allows us to perform an exploration of two new designs of the aeronautical injection system.

Proper Orthogonal Decomposition (POD) ; novel Gappy reduced order method ; Gappy-POD ; Non-parameterized geometrical variation ; hybrid approach ; Locally available data ; Galerkin projection ; dynamic extrapolation ; Navier-Stokes equations ; Large Eddy Simulation (LES) ; aeronautical injection system ; design exploration in industry ; efficiency ; robustness

1 Introduction

A large number of complex simulations of 3D unsteady and incompressible turbulent flows encountered in aeronautical engines, associated with different geometrical configurations, are crucial for designing new technologies. We consider the conception of the injection system in an aeronautical engine. We need multiple 3D incompressible and unsteady simulations of the non-reacting fluid flow in the primary zone of the combustor that occurs before the ignition point. These simulations are associated with different geometries of the injection system, so that the topology of the resulting incompressible and turbulent fluid flow could influence the flame stability in

the combustion zone of the gas turbine. This industrial process is challenging because of the size and the complexity of these numerical simulations. We propose to use reduced order modeling technologies to speed computational return times. Recently, we have proposed a new physical methodology to stabilize the classical POD-Galerkin Reduced Order Modeling (ROM) for the turbulent and incompressible Navier-Stokes equations, in order to cover a proper evolution of the Turbulent Kinetic Energy (TKE) spectrum and guarantee a conservation of the kinetic energy within the ROM, see Akkari et al. (2017, 2019). Nevertheless, if the proposed ROM is accurate for a given geometrical configuration, its accuracy is not guaranteed for complex geometrical variations, such as non-parameterized topological ones. The geometrical inaccuracy within a baseline reduced order model associated with a reference reduced order POD basis comes from the first POD mode corresponding to the mean velocity field. The velocity field needs to be predicted correctly in the entire domain, so that the Galerkin projection is predictible, for the new geometrical configuration. To remedy for this inaccuracy, we propose a novel approach based on the application of the Gappy- POD algorithm. The Gappy-POD has been first introduced in Everson and Sirovich (1995) as a technique for reconstruction of incomplete data field, assuming that the incomplete data vector represents a solution whose behavior can be characterized with an existing snapshots set. In T.Bui-Thanh et al. (2004), the POD technique was applied for inverse design purpose, in order to determine the optimal airfoil shape as an interpolation of known designs. In this paper, the POD technique was also applied in an iterative procedure in order to determine a POD associated with an incomplete pressure field on an airfoil at a given angle of attack. This iterative scheme was proposed for the first time in Everson et al. Everson and Sirovich (1995) for finding empirical eigenfunctions from the gappy data and it has been shown numerically that the method yields a spectrum and eigenfunctions that are close to those obtained from unmarred data. In Murray et al. Murray and Seiner (2008), the Gappy-POD was applied in order to complete velocity data obtained using particle image velocimetry, which is often marred by missing data in various spatial locations due to inconsistent seeding and other factors. The results demonstrate that the Gappy-POD can provide an estimate that is accurate within the experimental uncertainty of the measured data. In Csi et al. Csi and Ladeinde (2005), the Gappy-POD approach was performed on the inverse design of various airfoil shapes. In Raben et al. Raben et al. (2012), the Gappy-POD method was applied to replace erroneous measurements in digi-

tal particle velocimetry (DPIV), where a locally adaptive criterion allows for determination of the optimum number of POD modes required for the reconstruction of each replaced measurement. In Duan et al. Duan et al. (2012), the Gappy-POD was applied for aerodynamic shape optimization. In Mifsud et al. Mifsud et al. (2019), the Gappy-POD is used to fuse wind-tunnel measurements and computational fluid dynamics (CFD) data to provide a consistent and more comprehensive output of greater utility. In Jiang et al. Jiang et al. (2016), the Gappy-POD was applied in a sensor-CFD data fusion procedure for airflow field estimation.

Other than Gappy-POD methods have been proposed to deal with flows in variable geometries. Hay et al. Hay et al. (2010) have used the Lagrangian sensitivity with respect to shape parameters of a baseline POD basis, in order to compute subsequently a reduced order model at perturbed states. However, there is no guarantee these bases will be divergent free once mapped on any other geometry. This technique was applied for the 2D incompressible Navier-Stokes equations for a flow over a square cylinder. The considered mapping is the rotation of the cylinder. We cite also Freno and Cizmas (2014), where a POD method has been developed for modeling nonlinear flows with deforming meshes, thanks to dynamic functions that depend on parameters associated with flow unsteadiness.

In this work, we consider the turbulent and incompressible Navier-Stokes equations and we suppose a non-parameterized geometric variation locally in the fluid flow domain. We want to predict correctly and efficiently the velocity field in the scope of this new geometry, from a local high-fidelity computational knowledge available in a restricted fluid domain (RFD). This domain surrounds the geometrical modifications. A Gappy-POD is used as a first prediction step of the flow field in the scope of the new geometry defined by the interpolation of a pre-computed POD basis associated with one or several baseline high-fidelity simulations. The interpolation modal coefficients are determined via an optimization problem of the squared L^2-error between the available high-fidelity data around the non-parameterized geometric modification and the interpolation, evaluated only in the RFD. We will show that the interpolation assumption of the available data by the baseline POD basis vectors will be the origin of high point-wise errors on the velocity field topology in the scope of the new geometry, because of the non-parameterized geometrical changes. Indeed, the residual of the Gappy-POD optimization problem is far from being equal to zero in this case, due to the impossible interpolation of the new geometrical available data by a baseline

eigenbasis, which is of different topology. In order to correct these point-wise errors, we propose a second correction step which requires the local modification of the baseline POD basis vectors in order to fit the coherent structures of the local geometrical available physical data. The new basis vectors are termed updated modes. The residual of the optimization Gappy-POD problem will be equal to zero in this case. We precise that our proposed algorithm for the correction of the predicted missing data is efficient, because only one local POD performed with the local available data followed by a Gappy-POD is sufficient to correct and refine the topology of the fluid flow in the scope of the geometrical modification. Furthermore, it is important to precise that the local data around the geometrical modification is obtained thanks to the solution of a hybrid model coupling the restricted fluid domain to the reduced projection of the equations outside this domain. The coupling is an application of a penalization approach of the velocity field by setting a reference reduced order solution associated with a reference configuration as a physical fluid immersed boundary. This means that at the beginning we do not have access to any time and space information of the fluid flow in the new geometrical configuration, and we will access this information successively thanks to the hybrid approach and the newly proposed Gappy reduced order method.

The paper is organized as follows: in section 2, we briefly recall the Proper Orthogonal Decomposition technique. In section 3, we recall the Gappy-POD technique. In section 4, we give the mathematical framework of the POD-Galerkin projection of the 3D Navier-Stokes equations. In section 5, we show, for an incomplete 2D unsteady and laminar fluid flow, the impact of non-parameterized geometrical variation in the fluid domain on the accuracy of the classical Gappy-POD technique. In section 6, we propose our novel Gappy reduced order technique as discribed above. In section 7, numerical applications on a 2D laminar case and a 3D semi-industrial aeronautical injection system, are presented. This will enable us to perform a robust design exploration of this semi-industrial injection system with respect to non-parameterized geometrical variations in the swirler, such as the opening diameter of the primary zone of the combustor or the opening angle of this zone, with a speed up of the order of 100 with respect to a LES computation.

2 Proper Orthogonal Decomposition (POD)

We denote by $X = [L^2(\Omega)]^3$ the functional Hilbert space of the squared integrable functions over a bounded $3D-$open set Ω. The corresponding inner product is the one associated with the kinetic energy functional norm. They will be denoted respectively by $(.,.)$ and $\|.\|$. Consider $U(t) \in X$ the baseline velocity field of an unsteady incompressible flow, prior any geometrical modification. A reduced order POD subspace is obtained thanks to the snapshots method Sirovich (1987). More precisely, if we discretize the time interval to M points, then the snapshots set is given as follows: $\mathcal{S} = \{U(t_i) \;\; i = 1, ..., M\}$. The associated POD eigenmodes Φ_n, $n = 1, ..., M$, computed via the snapshots POD Sirovich (1987) start with the solution of the following eigenvalues problem given the temporal correlations matrix:

$$C_{ij} = (U(t_i), U(t_j)), \tag{1}$$

of size $M \times M$. We denote by $(A_n)_{n=1,...,M} = (A_{i,n})_{1 \leq i \leq M}$ and $(\lambda_n)_{n=1,...,M}$ for $n = 1, ..., M$, sets of respectively orthonormal eigenvectors and eigenvalues of the matrix C. Then, the POD-eigenmodes associated with λ_n, are given by:

$$\Phi_n(x) = \frac{1}{\sqrt{\lambda_n}} \sum_{i=1}^{M} A_{i,n} U(t_i, x) \;\; , \forall x \in \Omega \;\; \forall n = 1, ..., M. \tag{2}$$

3 Gappy-POD

By following Everson and Sirovich (1995), a mask has to be defined. Here, the support of this mask is the RFD where the POD modes of the baseline simulation are not consistent with the new geometry. If we denote by Ω_R the RFD, then:

- $n(x) = 1$ if $x \in \Omega_R$ ($U(t, G^{New})$ is known),
- $n(x) = 0$ otherwise ($U(t, G^{New})$ is unknown).

Where, we add the notation of "G^{New}" to a new physical quantity we need to compute in association with a new geometry, to differentiate it with the a priori baseline quantities that has been computed for a reference geometry. At this point, we suppose that we have access to the high-fidelity model for the new geometry G^{New} in Ω_R only: $U(t, G^{New})_{|\Omega_R}$

Now, given a baseline POD basis $(\Phi_i)_{i=1,...,M}$ with a baseline snapshots set associated with one or several geometries, then the predicted intermediate velocity field $\tilde{U}(t)$ for the new geometry is determined as follows in the Gappy-POD algorithm:

$$\tilde{U}(t, G^{New}, x) = \sum_{n=1}^{N} b_n(t, G^{New})\Phi_n(x), \tag{3}$$

where the interpolation POD coefficients b_n are determined by the following minimization of the instantaneous error between the interpolation (3) and the high fidelity solution, on Ω_R only:

$$\Big(b_1(t, G^{New}), ..., b_N(t, G^{New})\Big) = argmin_{\beta_1,\beta_2,...,\beta_N} \left\| \sum_{n=1}^{N} \beta_n(t)\Phi_n - U(t, G^{New})_{|\Omega_R} \right\|^2_{[L^2(\Omega_R)]^3}, \tag{4}$$

Finally, the complete predicted velocity field $U^{\text{predicted}}$ for the new geometry is obtained by:

- $$U^{predicted}(t, G^{New}, x) = U(t, G^{New}, x) \;\; if x \in \Omega_R. \tag{5}$$
- $U^{predicted}(t, G^{New}, x) = \tilde{U}(t, x)$ otherwise.

We recall that in (5), we supposed that we know $U(t, G^{New})$ restricted to Ω_R. We will propose in section 6.1.1 a procedure to derive a fastly computed prediction for $U(t, G^{New})_{|\Omega_R}$.

4 Model Order Reduction by POD

Let us denote by U^{ROM} the reduced approximation of the filtered field given by a LES model.

To achieve the POD reduced order modeling of the filtered incompressible Navier-Stokes equations, the approximated velocity field is expressed in the reduced order POD subspace:

$$U^{\text{ROM}}(t, x) = \sum_{n=1}^{N} a_n(t)\Phi_n(x), \;\; \forall x \in \Omega, \tag{6}$$

where, $N << M$ denotes the number of retained high energetic POD modes, and $a_1(t)$, $a_2(t)$,..., $a_N(t)$ are the temporal weights which are solutions of the following coupled dynamical system:

$$\begin{cases} \frac{da_n}{dt} + \left(div(U^{\mathrm{ROM}}(t) \otimes U^{\mathrm{ROM}}(t)), \Phi_n\right) = \nu \left(\Delta U^{\mathrm{ROM}}(t), \Phi_n\right) - \frac{1}{\rho} \left(\nabla p(t), \Phi_n\right) \\ \left(q, div(U^{\mathrm{ROM}}(t))\right)_{H^0} = 0 \quad , \forall q \in H^0 \\ a_n(0) = \left(\bar{U}(0), \Phi_n\right) \end{cases} \tag{7}$$

where div denotes the divergence operator, $p(t)$ is the pressure field, ρ the density, ν denotes the kinematic viscosity, $\bar{U}(0)$ is the initial condition of the velocity field and H^0 is the subspace of the divergence free X-functions.

We point out the fact that the equations upon which we perform the POD-Galerkin projection are the high-fidelity incompressible Navier-Stokes equations without any turbulence model and numerical scheme taken into account. However, the POD computation is associated with High-Fidelity snapshots $\bar{U}(t)$ obtained from LES of the Navier-Stokes equations.

In general, the first POD mode which describes the mean topology of the fluid flow is not kept and a ROM of the fluid dynamics equations represents only the fluctuating part. Here, POD modes are not restricted to the fluctuation part of $\bar{U}$, they also approximate the mean velocity. This could be very valuable because we are interested in using the reduced order modeling in order to predict the flow for new geometries Akkari et al. (2018). This enables the ROM to consider naturally the influence of the velocity fluctuations on the velocity mean.

So, we point out the following two remarks concerning our formulation of the reduced order modeling:

- The POD modes contain only the energetic scales of the flow. The dissipative scales at the Taylor macro-scale are not present in the basis.
- The flow rate in the flow domain is not guaranteed except if penalization is added in the pressure term to take into account the pressure difference between the inlet and the outlet.

We proposed in Akkari et al. (2017, 2019) to tackle these limits thanks to a physical stabilization by satisfying the kinetic energy budget. It is based on the enrichement of the POD-Galerkin ROM with the flow rate driving forces and with the most dissipative scales based on the velocity gradient.

We refer to Akkari et al. (2019) for more details concerning this enrichment strategy of the POD-Galerkin ROM.

This stabilization step is done because we need to have a reference POD basis which is rich enough to take into account the large features of scales in the case of turbulent and incompressible fluid flows. We will denote by Φ^E the dissipative basis. This is very important from the following two points of view:

- The reference dissipative POD basis constitutes a good candidate when applying the newly proposed Gappy reduced order method in order to reconstruct new incomplete snapshots set.
- The reference reduced order modeling obtained by the POD Galerkin projection of the Navier-Stokes equations upon the reference and enriched POD basis is stable in the sense of the kinetic energy conservation physical constraint. So, if we use the latter stable ROM in the hybrid approach as a physical boundary condition in order to compute the local data around the geometrical modification, it guarantees the stability of the LES with global penalization of the velocity field with the reference reduced order solution by POD-Galerkin.

5 Limits of the classical Gappy-POD in our setting

In this section, we illustrate the limits of the Gappy-POD for our particular application. Suppose that we have the access to one or several high fidelity aerodynamic simulations corresponding to one or several geometric configurations, as shown on Figures 1 and 2.

Figure 1: On the left, a channel configuration with an obstacle on the upper and lower walls. On the right, a channel configuration with a new obstacle at this time, translated with respect to the first one in the horizontal direction, and with a new length

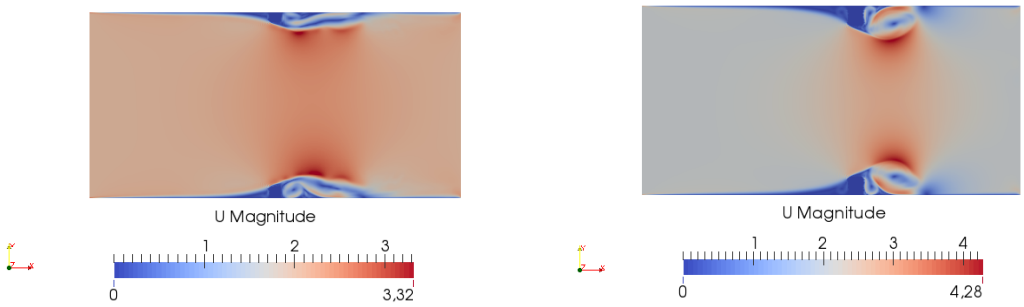

Figure 2: On the left, a velocity field snapshot in the channel configuration with an obstacle on the upper and lower walls. On the right, a velocity field snapshot in the channel configuration with a new obstacle see Figure 1.

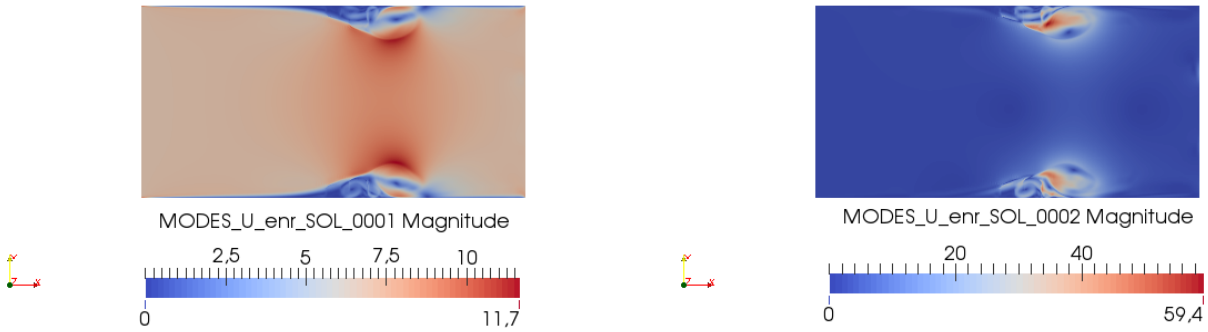

Figure 3: On the left, Φ_1^E the first POD mode with the enriched snapshots set. On the right, Φ_2^E the second POD mode with the enriched snapshots set

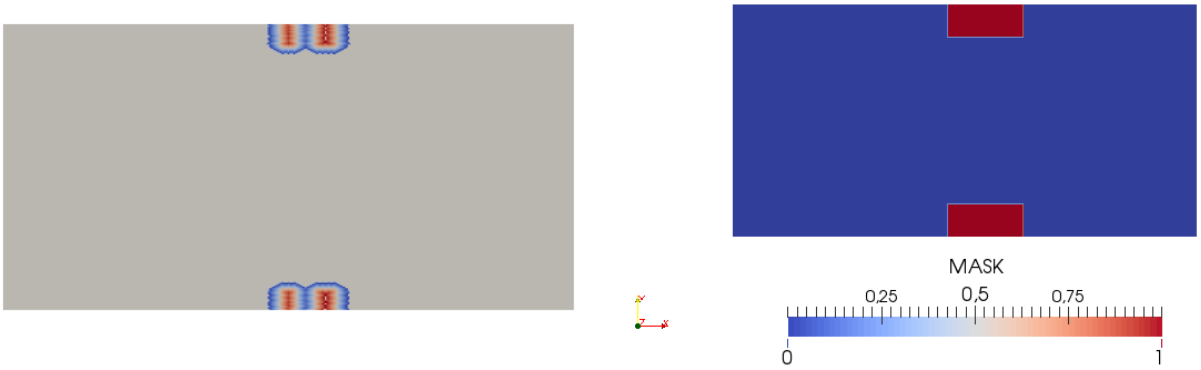

Figure 4: On the left, a channel configuration with two obstacles on the lower and upper walls situated respectively at the same position of the above ones, but with a new intermediate length and two different widths. On the right, a mask vector describing the restricted fluid domain Ω_R of the new solution by the red color, and the unknown flow field data zone by the blue color

Let $\left(\Phi_i^E\right)_{i=1,\ldots,N}$ be the POD basis (Figure 3) with the baseline instantaneous snapshots set where all the snapshots are completely known.

Let $U(t, G^{New})$ (see Figures 4 and 6) be another solution vector with a new configuration. We have two classical ways to build the fluid velocity field associated with the new technology: 1) either we apply directly an order reduction of the Navier-Stokes equations upon the POD basis associated with the baseline snapshots. Then, it is clear that the baseline POD basis functions will fail to characterize the flow data close to the new geometry. We note from Figure 3 that the enriched POD modes have a non-zero velocity of the fluid flow even in the obstacles associated with each ones of the baseline test cases shown on Figure 2. Hence, these POD velocity modes could not be used in a confident way to model correctly a new geometrical fluid flow. 2) Another possibility is to apply a Gappy-POD procedure if we have the access to some high-fidelity informations with the corresponding mask n, as shown on Figure 4.

The complete predicted velocity field $U^{\text{predicted}}(t, G^{New})$ by Gappy-POD for the new geometry is shown on Figure 5, and the associated high-fidelity solution in 6.

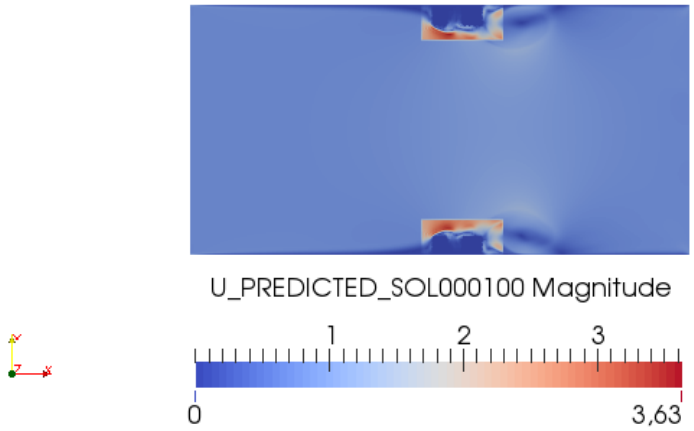

Figure 5: Final time step predicted flow field $U^{\text{predicted}}(T, G^{New})$ by Gappy-POD

It is clear when compared to the high-fidelity model solution, that the Gappy-POD under estimates the velocity field in the fluid domain. This could be explained because the baseline POD modes are not interpolant

within the local zoom in red defined by the mask vector. The associated absolute nodal errors with respect to the high fidelity aerodynamic field in the direction of the abscissa axis, scaled by the inlet velocity value, are shown on Figure 7. We detail our new procedure in the following section, that is able to take into account such geometrical variations.

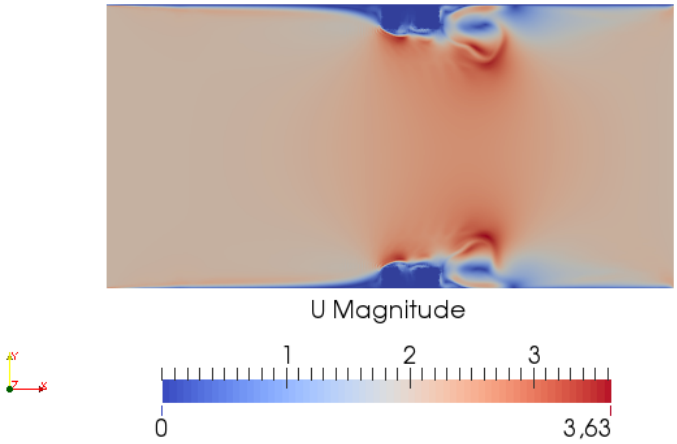

Figure 6: $U(t, G^{New})$: Final time step 2D laminar incompressible flow in a channel, given a constant inlet velocity on the channel inlet, an outlet boundary condition on the channel outlet and a wall boundary condition on the upper and lower walls of the channel

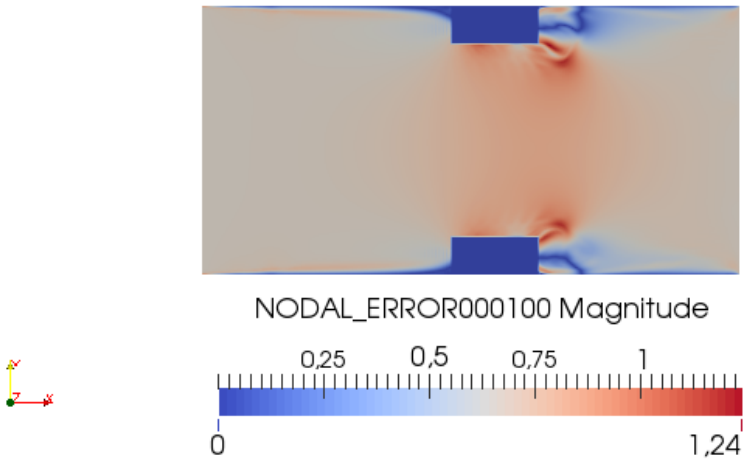

Figure 7: $\frac{|U_1(t,x,G^{New}) - U_1^{\text{predicted}}(t,x,G^{New})|}{U_{inlet}}$

6 Proposition of a new algorithm

6.1 Newly proposed Algorithm

6.1.1 Hybrid approach: Local High Fidelity solution/Global reduced order solution

We will begin our fluid flow computation by applying a hybrid approach as illustrated on Figure 8. We set in the scope of the new geometry of the fluid domain the velocity field as a fluid immersed boundary condition defined by the solution of a baseline reduced order model associated with a baseline fluid flow that has been computed once and for all in association with a reference geometrical domain. The global zone defined by a reference fluid flow is forced around the local zone as a penalization. In the local zoom we run the finite volume high-fidelity equations of the Navier-Stokes model. We precise that the reference reduced order solution is saved on a coarser grid for $\Omega \setminus \Omega_R$ (see Figure 8) in order to gain efficiency when computing the pressure field during the hybrid simulation along the global fluid domain. We denote U^{hybrid} the velocity field obtained by this approach.

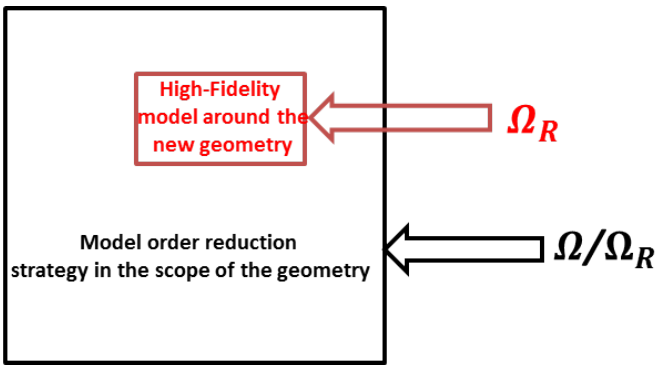

Figure 8: Schematic representation of the hybrid approach

6.1.2 Newly proposed Gappy reduced order method

We will apply a new Gappy reduced order method in order to compute a calibrated velocity field in the wake of the new geometry. We want to benefit from the knowledge of the local high-fidelity solution by the hybrid approach. Hence, we perform the following steps:

1. We define updated modes Ψ_n from the local modification of the reference ones in such a way to include the coherent structures of the newly computed local high-fidelity solution by the hybrid approach. These updated modes are obtained thanks to the following steps:

   - Compute the complete fields $U^{\text{predicted}}(t, x, G^{New})$ with the classical Gappy-POD approach (4). We precise that the Gappy-POD modes Φ_n in (4) are here the reference POD modes Φ_n^E projected on the coarse mesh of the fluid zone $\Omega \setminus \Omega_R$.
   - Computation of a new POD basis associated with the previous reconstructed aerodynamic fields $U^{\text{predicted}}(t, x, G^{New})$: $\Psi_n(x) = \frac{1}{\sqrt{c_n}} \sum_{i=1}^{M} \mathcal{C}_{i,n} U^{\text{predicted}}(t_i, x, G^{New})$, where $(\mathcal{C}_n)_{n=1,\dots,M}$ are the eigenvectors of the correlations matrix defined by: $(U^{\text{predicted}}(t_i, G^{New}), U^{\text{predicted}}(t_j, G^{New}))_{[L^2(\Omega)]^3}$, and $(c_n)_{n=1,\dots,M}$ is the sequence of the associated eigenvalues.

2. Galerkin projection step of the Navier-Stokes equations (still with no modelling of the turbulence) over the new POD basis Ψ_n: $\vec{c}(t, G^{New})$

are the temporal coefficients of the Galerkin projection of the Navier-Stokes equations upon Ψ_n.

- $U^{ROM}(t,x,G^{New}) = U^{\text{hybrid}}(t,x,G^{New})$ if $x \in \Omega_R$.
- $U^{ROM}(t,x,G^{New}) = \sum_{n=1}^{N} c_n(t,G^{New})\Phi_n^E(x)$ otherwise, where Φ_n^E are the reference global POD modes defined on the refined reference grid.

It is important to note that the modes Ψ_n are mainly with local support Ω_R and are the locally updated modes defined in step 1 by the coherent structures obtained by data compression of the snapshots set $\left\{U^{\text{hybrid}}(t,x,G^{New}),\ \ x \in \Omega_R\right\}$. Hence, the latter temporal coefficients $c_n(t,G^{New})$ describe mainly the dynamics of the new hybrid local high-fidelity solution defined on Ω_R. Moreover, it is important to notice that the new Gappy reconstruction is done as usual following Φ_n^E but with temporal coefficients $c_n(t,G^{New})$ that on the contrary to the Gappy-POD will describe the dynamics of the new hybrid local high-fidelity solution defined on Ω_R.

We would like to summarize the notations we used until now in the paper: this could be useful for the following part.

- U: the nominal HF solution.
- $U^{\text{hybrid}}(G^{New})$: obtained by the immersed boundary technique (see section 6.1.1). By construction $U^{\text{hybrid}}(G^{New})_{\Omega\setminus\Omega_R} = U$.
- $\tilde{U}(G^{New})$: Gappy-POD reconstruction (3).
- $U^{\text{predicted}}(G^{New})$: Gappy-POD prediction.
- $U^{ROM}(G^{New})$: New ROM prediction (see section 6.1.2).

6.2 A consistency result of the newly proposed algorithm

We propose a consistency result of our newly proposed approach that shows that the error related with the application of this algorithm when no geometrical variation occurs, is equal to zero.

Proposition 1 *The newly Gappy reduced order approach proposed in section 6.1.2 is consistent: if no geometrical modification is introduced, then the ROM solution in step 2 is identical to the one obtained by the reduced order model* (7) *upon the dissipative basis* Φ^E *, under the following assumption: the reference POD modes* Φ_n^E *are orthogonal with respect to the gappy inner product* $(.,.)_{[L^2(\Omega_R)]^3}$.

Proof 1 *Without geometrical modification* $U(G^{New}) = U = U^{\text{hybrid}}$.

There exists $N \leq M$ *such that* $\forall \quad i = 1, ..., M$, $\left\| U(t_i) - \sum_{n=1}^{N} (U(t_i), \Phi_n^E)_{[L^2(\Omega)]^3} \Phi_n^E \right\|^2_{[L^2(\Omega)]^3} = M \times 0$. *In particular, this squared difference is zero on* $\Omega_R \subset \Omega$*:* $\forall \quad i = 1, ..., M$, $\left\| U(t_i) - \sum_{n=1}^{N} (U(t_i), \Phi_n^E)_{[L^2(\Omega)]^3} \Phi_n^E \right\|^2_{[L^2(\Omega_R)]^3} = 0$. *Hence, thanks to the fact that the reference POD modes are orthogonal using the Gappy inner product* $(.,.)_{[L^2(\Omega_R)]^3}$*, the unique solution of* (4) *for* $\Phi = \Phi^E$ *is* $b_n(t_i, G^{New} = G^{ref}) = (U(t_i), \Phi_n^E)_{[L^2(\Omega)]^3}$. *Then* $\tilde{U}(t) = \sum_{n=1}^{N} (U(t_i), \Phi_n^E)_{[L^2(\Omega)]^3} \Phi_n^E = U(t)$. *Hence* $U^{\text{predicted}} = U$*, and the POD basis on these snapshots are identical, namely* Φ^E *and* Ψ *are identical.*

The proof was based on the fact that the Gappy-POD on the fluid region Ω_R is accurate because it is performed with the dissipative POD basis Φ^E associated with the same complete data over Ω that has been restricted to Ω_R.

7 Numerical framework and experiments

7.1 Flow solver

For the presented simulations, the low-Mach number solver YALES2 Moureau et al. (2011a) for unstructured grids is retained. This flow solver has been specifically tailored for the direct numerical simulation and large-eddy simulation of turbulent reacting flows on large meshes counting several billion cells using massively parallel super-computers Moureau et al. (2011b); Malandain et al. (2013). The Poisson equation that arises from the low-Mach formulation of the Navier-Stokes equations is solved with a highly efficient Deflated Preconditioned Conjugated Gradient method Malandain et al. (2013).

7.2 3D turbulent and unsteady incompressible semi-industrial test case

7.2.1 Test case presentation

In what follows, we apply our new approach for a 3D unsteady, turbulent and incompressible fluid flow in a fuel injection system. The main objective is to be able to have an efficient strategy for the computation of the aerodynamic field in the primary zone of the combustion chamber. The Preccinsta test case Meier et al. (2007); Weigand et al. (2005) is presented in Figure 9. This lean-premixed burner has been widely studied in the combustion community to validate large-eddy simulation models Moureau et al. (2011b); Lartigue et al. (2004); Roux et al. (2005); Moureau et al. (2007); Fiorina et al. (2010); Franzelli et al. (2012); Lourier et al. (2017).

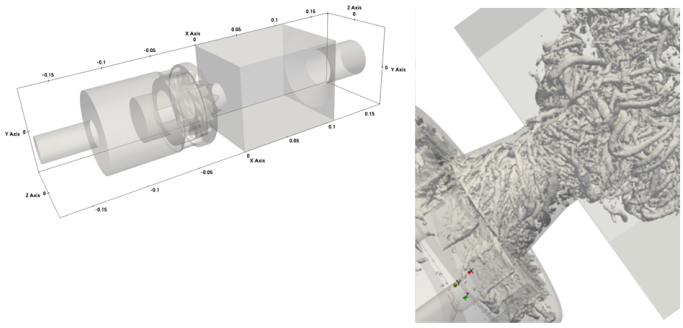

Figure 9: The 3D unsteady turbulent and incompressible flow in a fuel injection system and in the primary zone of the combustion chamber, given a constant inlet velocity, an outlet boundary condition on the channel outlet and a wall boundary condition on the upper and lower walls of the channel.

The 3D turbulent flow in the complex configuration presented in Figure 9 is considered. The kinematic viscosity $\nu = 10^{-5}\,\mathrm{m}^2/\mathrm{s}$ yields a Reynolds number $45,000$ based on the inlet velocity and the length of the duct. The presented high-fidelity simulation with 14 million tetrahedra runs over 512 cores during 5 days in order to obtain a physical simulation time equal to 250 ms. In order to build the dissipative reduced basis, 2500 snapshots of the solution are taken, extracted at each time step of the original high-fidelity simulation. We point out the fact that these 2500 snapshots are taken from 6644 time steps of the high-fidelity simulation corresponding to the final 25

ms of its total physical time.

7.2.2 Construction of a reference POD basis

As explained in the previous sections, we first need to construct a reference POD basis which is rich enough to take into account the large features of scales in the case of turbulent and incompressible fluid flows. This reference POD basis is obtained in this semi-industrial case of the Preccinsta burner, in association with snapshots data generated from only one LES high-fidelity simulation of the Navier-Stokes equations with the reference geometrical configuration presented in Figure 9. We show that our newly proposed geometrical adaptive procedure is robust with only one complete High-Fidelity simulation, the baseline simulation, and one dissipative large scale reduced order basis in association. All the detailed informations concerning the dissipative reduced order basis construction can be found in Akkari et al. (2019).

The velocity-based and gradient velocity-based POD modes were computed through a snapshots POD. The CPU ressources needed for this computation are 768 cores, to guarantee a memory availability to read the 2500 time snapshots. The computation runs during 6 hours for the velocity-based POD modes and 9 hours for the gradient velocity-based POD modes. However, these operations were not well distributed over the 768 cores due to the following issue: in YALES2, the post-processing would lead to at least one file per snapshot. In this case, a temporal snapshot was not post-processed as one file per subdomain, i.e. the number of solution files per time step was less than the number of mesh partitions which is 128 in this case. This is due to the limited number of files that we might save on the super computer, especially when considering 2500 snapshots.

By applying the dissipative POD approach, we get a new velocity-based reduced order basis as shown from Figure 10 until Figure 21. The enforcement of the small scales is done starting from the 5^{th} mode in the reduced order basis. The new velocity-based modes Φ_5^E, Φ_6^E, Φ_7^E, $\Phi_8^E, ..., \Phi_{12}^E$ show very large features of spatial scales which were not observed within the classical POD modes. Moreover, the largest scales exhibit local structures in the fluid domain which are the small vortices carrying out the dissipative energy, by analogy with the gradient velocity-based POD modes (see Akkari et al. (2019) for more details concerning the dissipative reduced basis construction).

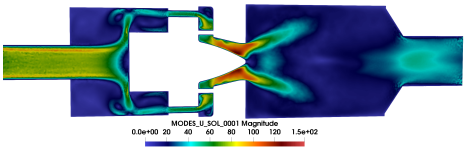

Figure 10: Velocity mode $\Phi_1^E = \Phi_1$. Akkari et al. (2019)

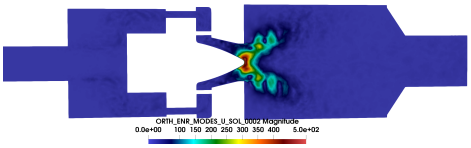

Figure 11: Velocity mode $\Phi_2^E = \Phi_2$. Akkari et al. (2019)

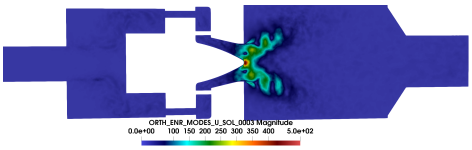

Figure 12: Velocity mode $\Phi_3^E = \Phi_3$. Akkari et al. (2019)

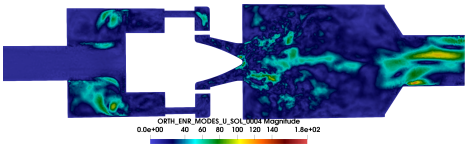

Figure 13: Velocity mode $\Phi_4^E = \Phi_4$. Akkari et al. (2019)

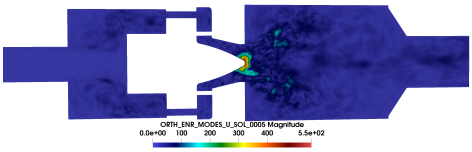

Figure 14: Velocity mode Φ_5^E. Akkari et al. (2019)

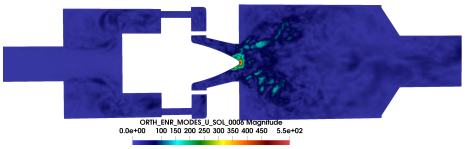

Figure 15: Velocity mode Φ_6^E. Akkari et al. (2019)

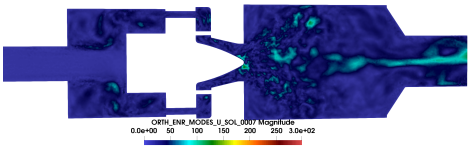

Figure 16: Velocity mode Φ_7^E. Akkari et al. (2019)

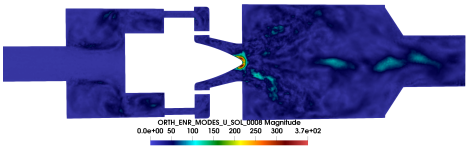

Figure 17: Velocity mode Φ_8^E. Akkari et al. (2019)

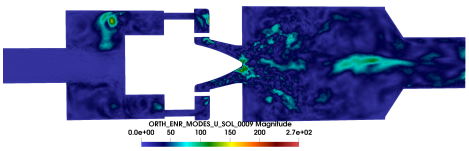

Figure 18: Velocity mode Φ^E_9. Akkari et al. (2019)

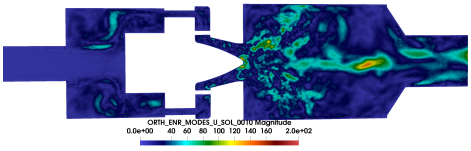

Figure 19: Velocity POD mode Φ^E_{10}. Akkari et al. (2019)

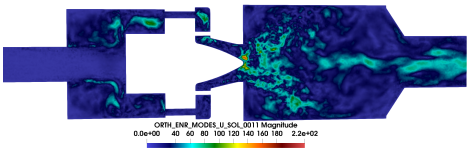

Figure 20: Velocity mode Φ^E_{11}. Akkari et al. (2019)

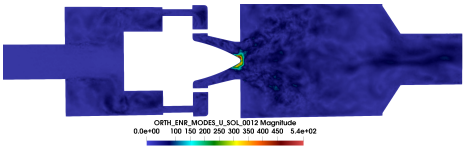

Figure 21: Velocity mode Φ^E_{12}. Akkari et al. (2019)

7.2.3 Introducing new geometric configurations

Two new configurations of the injection system are introduced, see Figure 22.

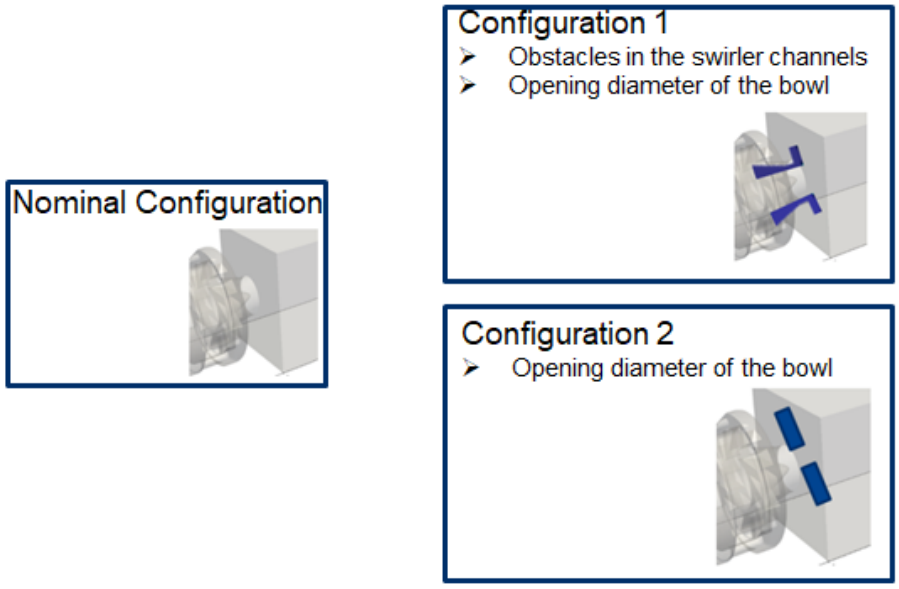

Figure 22: Two new configurations are considered by introducing solid obstacles in the swirler's zone. These obstacles are defined using level set functions. We point out the fact that our geometrical modifications are non-parameterized because the level set functions are not necessarily defined by a parametric function but rather by a "if loop" that delimits the spatial location of the immersed solid boundary.

We will apply our newly proposed algorithm in order to determine for each of these two configurations, the new fluid flow topology and the new recirculation zones in a robust and efficient fashion.

7.2.4 Hybrid approach: Local High Fidelity solution/Global reduced order solution

As mentioned in section 6, the first step of our newly proposed algorithm is to compute locally the new geometrical velocity field in a restricted fluid domain that is identified by a mask, see Figure 23.

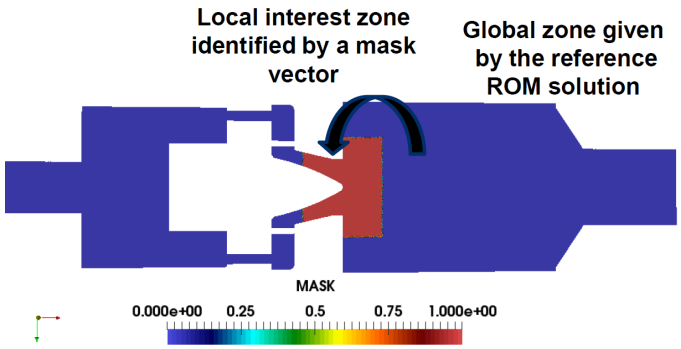

Figure 23: Mask vector that defines the local zone in red Ω_R of interest around the geometrical variations. In blue the global zone $\Omega \setminus \Omega_R$.

The result of the hybrid approach is illustrated see Figure 24, when applied to the first configuration of Figure 22. The physical time needed in order to obtain a solution with good statistics is far less than the time we fixed in this case which is 21 ms. This physical time is ten times greater than the flow through time associated with the zoom box in red. Therefore, the maximal CPU time needed in order to perform the LES in the local zone in red is in this case 3.5 hours on 128 cores. We have a very important reduction in the CPU time needed for this local LES with respect to the complete LES, as a consequence of the reduction of the computation domain. The remainder of the fluid domain is defined by the reference reduced order velocity field associated with the reference configuration, which has been saved on a coarser grid for the region $\Omega \setminus \Omega_R$. We finally point out the fact that the pressure field is computed all over the fluid domain by the High-Fidelity solver, because our reference dissipative reduced order model does not contain the pressure field. The pressure computation in the hybrid simulation is efficient as we did a derefinement step by 30 percent for the reference dissipative velocity modes in the global zone $\Omega \setminus \Omega_R$ in blue, see Figure 23. In other words, the dissipative velocity modes, see Figure 10 until Figure 21, are saved on a coarser grid in the blue zone of Figure 23.

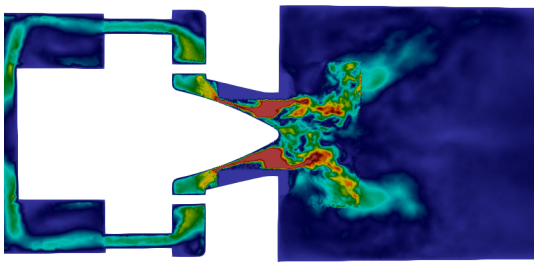

Figure 24: An unsteady solution field of the hybrid simulation: the inlet boundary conditions for the local high-fidelity solution are well reproduced.

The flow must be determined in the wake of the new swirler. In what follows, we apply our newly proposed Gappy reduced order method in order to adapt the fluid flow topology outside the red box of Figure 23 for it to follow the geometrical variation of the swirler.

7.2.5 Application of the newly proposed Gappy reduced order method for the two new configurations

We now apply the proposed Gappy reduced order method in section 6 to the new two configurations, see Figures 25 and 26 respectively, then we get the reduced order model coefficients associated respectively with these locally updated modes and the calibrated entire mean flow fields with respect to the geometrical variation, are represented in Figure 33 and 34. We precise that the computation of the updated POD basis Ψ was done in a completely distributed fashion by processing all the predicted snapshots as one file per subdomain which yields 128 files. Indeed, we were able to save the predicted snapshots by Gappy-POD in one HDF5 file as the Gappy-POD is performed outside the high-fidelity solver, so we are able to control the data processing. Hence, the distributed Snapshots POD over a multiple of 128 cores will be able to read effciently a large number of snapshots (2500 in this case) per subdomain i.e. per CPU process.

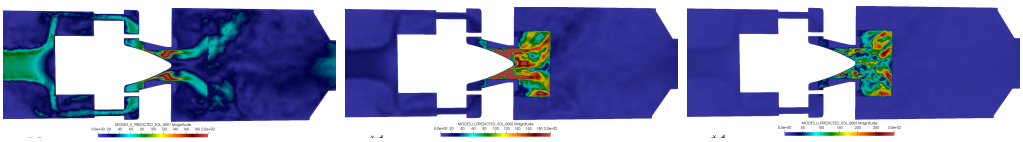

Figure 25: Locally updated velocity modes Ψ_1,Ψ_2, Ψ_3, Ψ_4, Ψ_5 and Ψ_6 with respect to the local high-fidelity solution associated with the first configuration. Few modes are of global support Ω and many have a local support Ω_R.

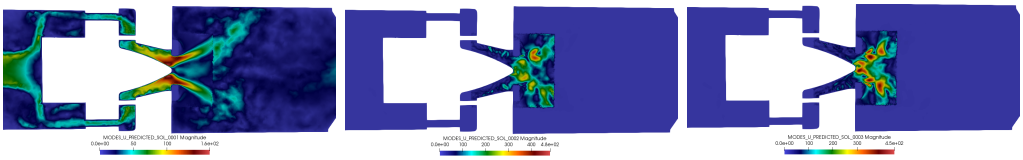

Figure 26: Locally updated velocity modes Ψ_1,Ψ_2, Ψ_3, Ψ_4, Ψ_5 and Ψ_6 with respect to the local high-fidelity solution associated with the second configuration. Few modes are of global support Ω and many have a local support Ω_R.

The ROM coefficients resepctively with the locally updated modes for the two new configurations are shown on Figures 27, 28, 29, 30, 31 and 32.

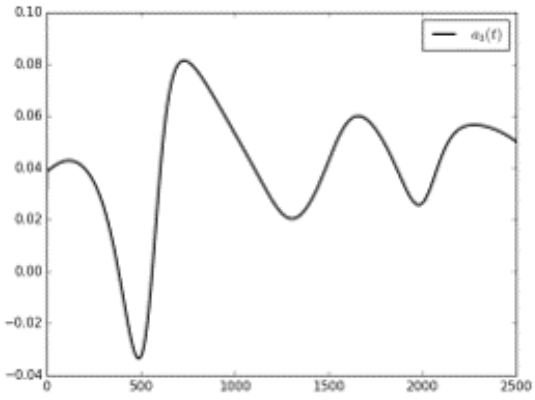

Figure 27: $c_1(t, G^1)$.

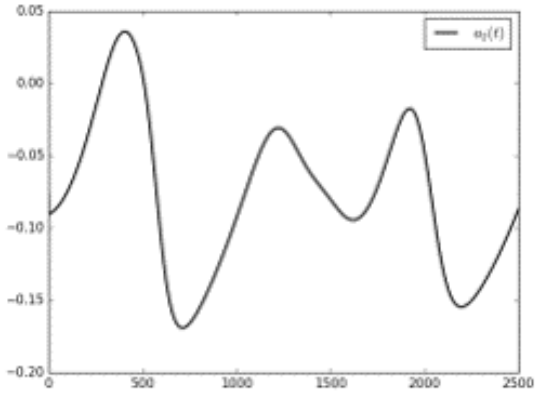

Figure 28: $c_2(t, G^1)$.

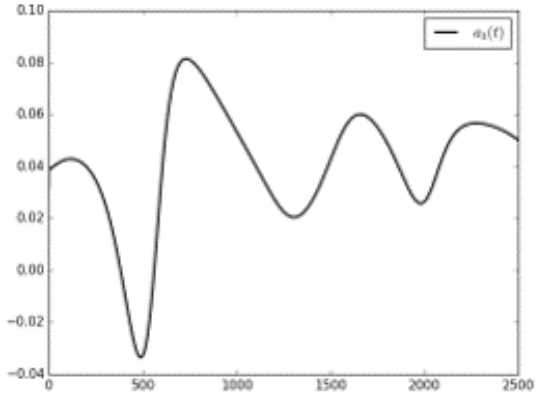

Figure 29: $c_3(t, G^1)$.

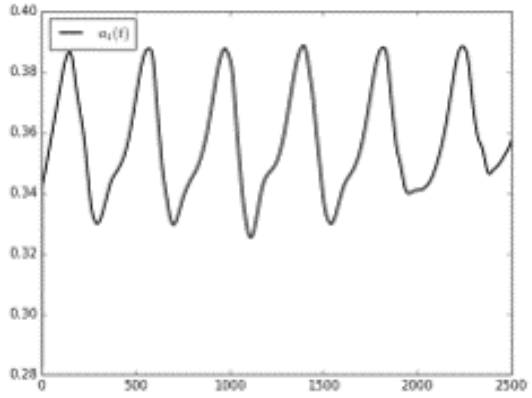

Figure 30: $c_1(t, G^2)$.

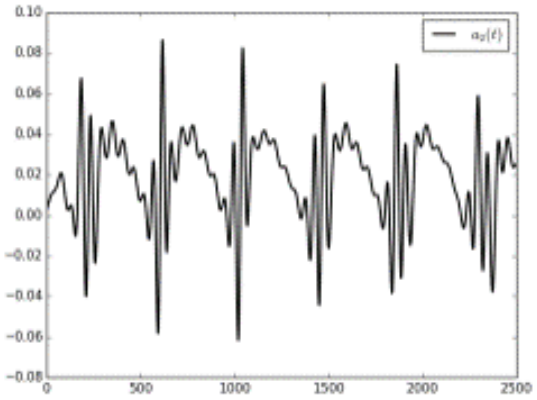

Figure 31: $c_2(t, G^2)$.

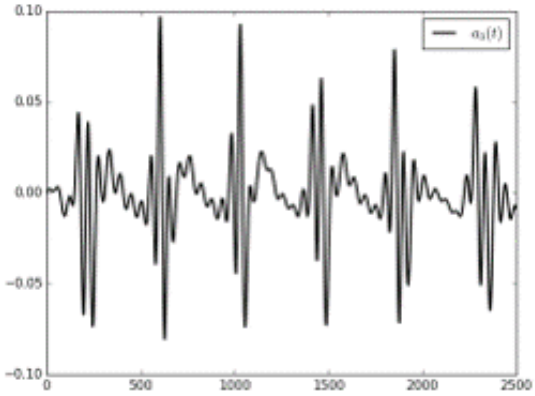

Figure 32: $c_3(t, G^2)$.

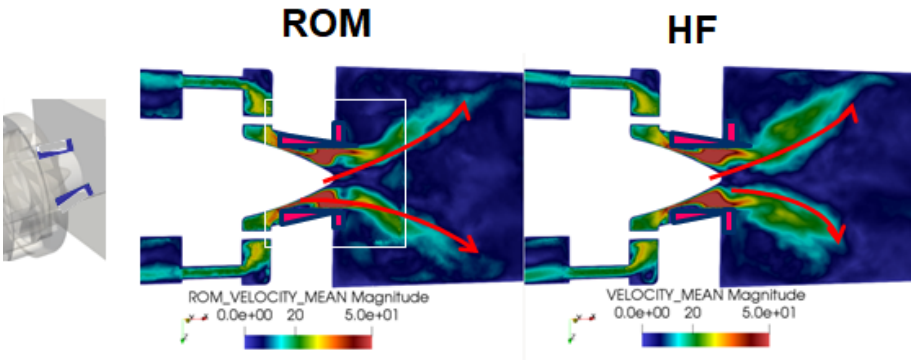

Figure 33: The new geometrical mean velocity fields for the first new geometry.

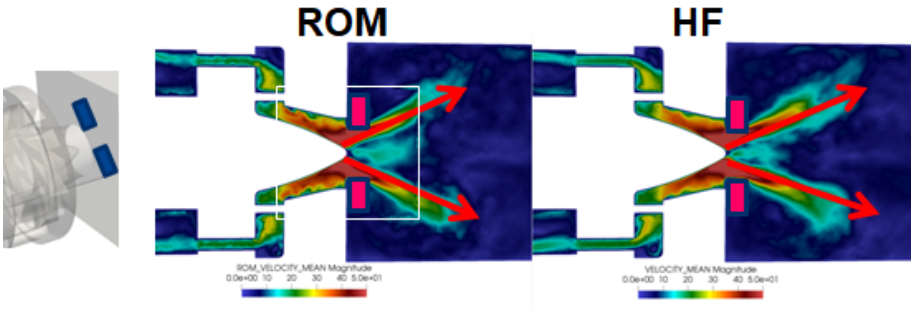

Figure 34: The new geometrical mean velocity fields for the second new geometry.

7.2.6 Specification for the design in combustion: A posteriori verification of the ROM quality on a 1D quantity of interest

In what follows we show the recirculation zones of each one of the two mean fields with the two new configurations, given by the new Gappy approach and the complete LES. These recirculations zones are the same in reacting and non reacting cases. In order to plot these recirculation zones, we consider three axes in the fluid domain along the y-direction for $z = 0$ and for different $x-$ positions outside the RFD, in order to compare our new gappy reduced order strategy with the result of the LES, see Figure 35. We add also to these validation results, a comparison with the recirculation zones obtained when the classical Gappy-POD approach is applied outside the reduced fluid domain. All these results are summarized on Figures 36, 37, 38, 39, 40 and table 1:

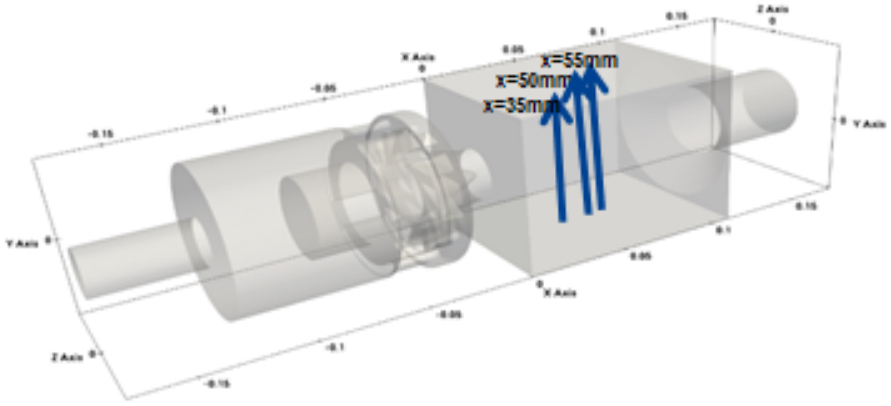

Figure 35: The three $y-$axes for the recirculation zones

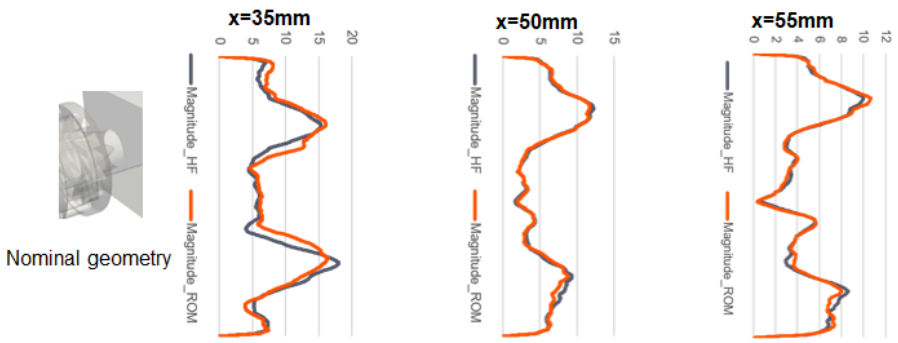

Figure 36: Reference geometry: comparison of the recirculation zones obtained respectively as a consequence of the dissipative Galerkin ROM by Φ^E in orange and the HF LES in black

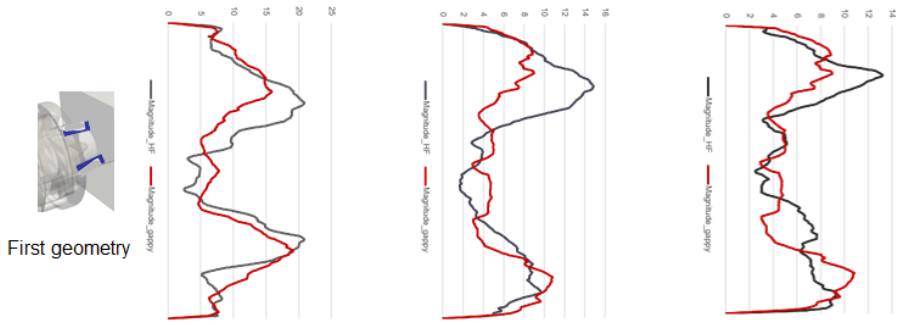

Figure 37: First new geometry: comparison of the recirculation zones obtained respectively as a consequence of the classical Gappy-POD in red and the HF LES in black

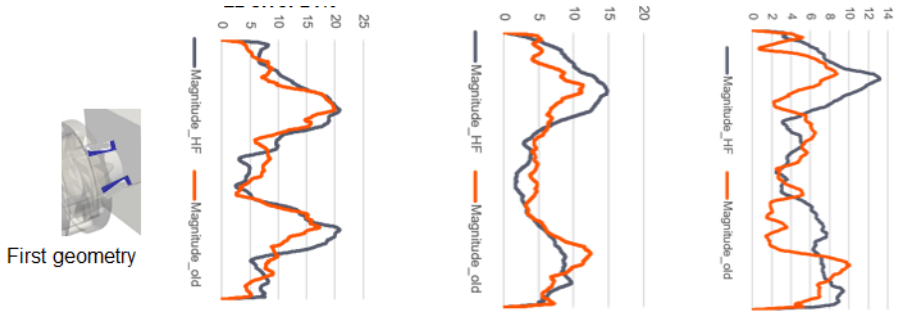

Figure 38: First new geometry: comparison of the recirculation zones obtained respectively as a consequence of the geometrical reduced order strategy in orange and the HF LES in black

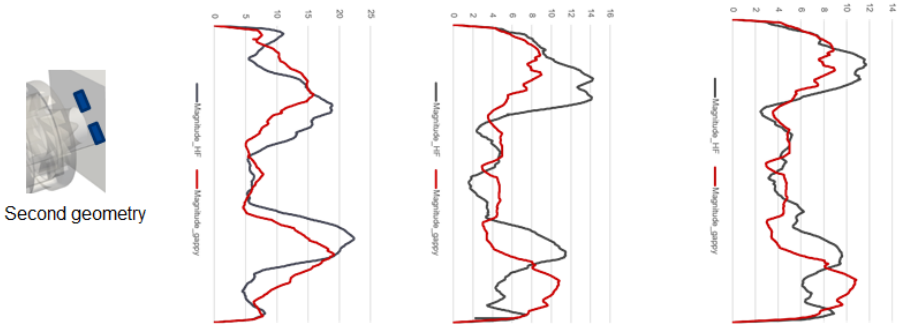

Figure 39: Second new geometry: comparison of the recirculation zones obtained respectively as a consequence of the classical Gappy-POD in red and the HF LES in black

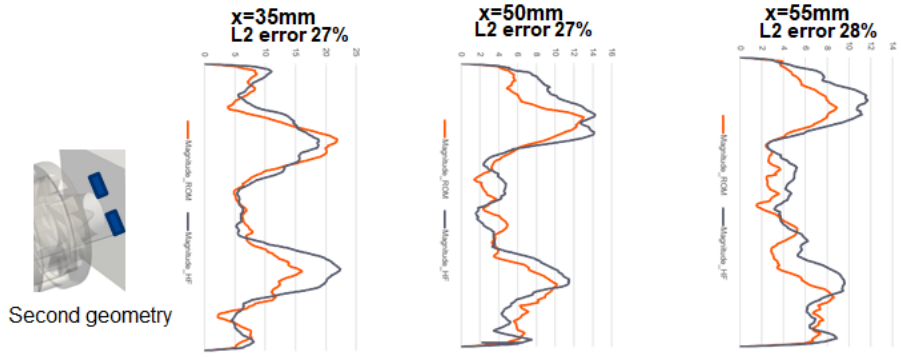

Figure 40: Second new geometry: comparison of the recirculation zones obtained respectively as a consequence of the geometrical reduced order strategy in orange and the HF LES in black

We propose in what follows two different criteria in order to evaluate the quality of the new gappy approach to recover the mean velocity field with respect to the complete LES.

1. The position of the recirculation zones with respect to each one of the two walls of the aeronautical injector. If we denote by $v(y)$ a velocity value along the corresponding $y-$axis, then this position is defined on each wall side by:

$$y_g = \frac{\int y(v(y) - \bar{v})dy}{\int (v(y) - \bar{v})dy},$$

as we can see on Figure 41. Then, we compute respectively the two relative errors with respect to the position of the two recirculation zones within the LES.

2. The L^2-relative error with respect to the LES on each 1D $y-$axis.

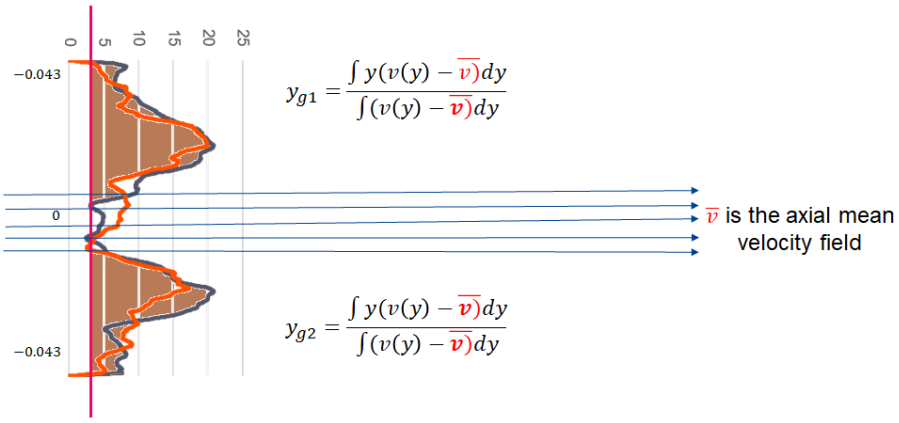

Figure 41: Illustration of the positions of the two recircluation zones on each wall side

The results are shown in Tables 1, 2.

Table 1: Evaluation of the 1D L^2-relative errors along the three $y-$axis respectively.

Geometry and $y-$axis	**Gappy-POD**	**New Gappy approach**
First new geometry: $x = 35$ mm	32%	24%
Second new geometry: $x = 35$ mm	36%	27%
First new geometry: $x = 50$ mm	41%	34%
Second new geometry: $x = 50$ mm	50%	27%
First new geometry: $x = 55$ mm	31%	46%
Second new geometry: $x = 55$ mm	32%	28%

Table 2: Evaluation of the position of the recirculation zones of the two new geometries and their relative errors, Err1 for our method and Err2 for the Gappy-POD, with respect to the LES ones.

Config.	**HF**	**New Gappy**	**Gappy-POD**	**Err1**	**Err2**
Geo1: $x = 35$ mm	$y_{g1} = -0.0211$	$y_{g1} = -0.019$	$y_{g1} = -0.0246$	6%	16%
Geo1: $x = 35$ mm	$y_{g2} = 0.022$	$y_{g2} = 0.020$	$y_{g2} = 0.023$	6%	6%
Geo1: $x = 50$ mm	$y_{g1} = -0.0256$	$y_{g1} = -0.024$	$y_{g1} = -0.031$	5%	22%
Geo1: $x = 50$ mm	$y_{g2} = 0.03$	$y_{g2} = 0.028$	$y_{g2} = 0.032$	6%	9%
Geo1: $x = 55$ mm	$y_{g1} = -0.027$	$y_{g1} = -0.024$	$y_{g1} = -0.031$	10%	14%
Geo1: $x = 55$ mm	$y_{g2} = 0.028$	$y_{g2} = 0.031$	$y_{g2} = 0.032$	10%	13%
Geo2: $x = 35$ mm	$y_{g1} = -0.021$	$y_{g1} = -0.020$	$y_{g1} = -0.024$	5%	15%
Geo2: $x = 35$ mm	$y_{g2} = 0.0195$	$y_{g2} = 0.0197$	$y_{g2} = 0.0234$	0.9%	19%
Geo2: $x = 50$ mm	$y_{g1} = -0.027$	$y_{g1} = -0.025$	$y_{g1} = -0.031$	8%	14%
Geo2: $x = 50$ mm	$y_{g2} = 0.023$	$y_{g2} = 0.026$	$y_{g2} = 0.032$	16%	41%
Geo2: $x = 55$ mm	$y_{g1} = -0.029$	$y_{g1} = -0.028$	$y_{g1} = -0.031$	4%	6%
Geo2: $x = 55$ mm	$y_{g2} = 0.027$	$y_{g2} = 0.031$	$y_{g2} = 0.032$	16%	20%

We remark first that when no geometrical modification is introduced, see Figure 36, the ROM velocity field is exactly the one obtained by the complete LES. We remark also that the newly proposed geometrical Gappy reduced order approach allows the reduced order solution to follow the real topology of the fluid flow in the global zone of the domain, after non-parameterized geometrical modifications. We see that the reduced order solution respects the recirculation zones of the fluid flow, see Figures 38 and 40, and table 2. These recirculation zones are different from the baseline configuration, see Figure 36. We see also that the classical Gappy-POD approach does not provide accurate results neither in the sense of the recirculation zones, nor in the sense of the 1D L^2-relative errors all along the three $y-$ axis respectively as shown in table 1.

7.2.7 CPU time reduction

In Table 3, we evaluate the efficiency of the newly proposed Gappy reduced order approach with respect to the high- fidelity simulation.

It is important to note that the step which is the most CPU-consuming in the proposed approach is the hybrid computation by global penalization of the velocity field: the pressure field is still computed all over the fluid

domain, so an effort has been done by coarsening the grid in the scope of a new geometry. We reached a maximum CPU time equal to 3.5 hours on 128 cores.

Table 3: Total computational cost.

Operation	**Wall Clock Time**
High-fidelity YALES2 solver (512 cores)	5 days
High-fidelity over Ω_R (128 cores)	3.5 hours
Classical Gappy-POD on Ω_R (512 cores)	3 min
Distributed POD Ψ with the predicted fields $U^{predicted}(t, G^{New})$ (512 cores)	3 min
Galerkin projection of the Navier-Stokes equations upon Ψ (512 cores)	3 min
Resolution of the reduced equations (1 core)	3.7 sec
Speed up factor	100

7.3 2D laminar and unsteady incompressible test case

7.3.1 Application of the newly proposed Gappy reduced order method

Now we apply the newly proposed approach to the laminar $2D$ case where we identified some limits of the classical Gappy-POD approach to tackle geometrical variations in section 5. The new geometrical entire flow data is now illustrated on Figure 42.

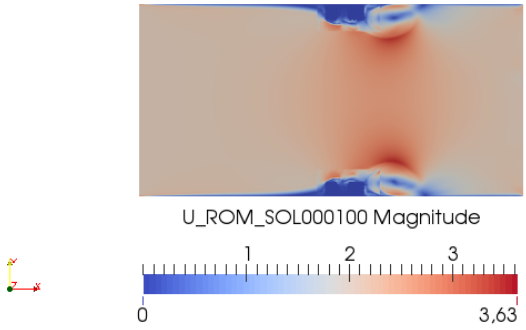

Figure 42: Final time step corrected flow field $U^{\mathrm{ROM}}(t, G^{New})$ by the newly proposed Gappy reduced order approach

The associated absolute nodal errors with respect to the high-fidelity aerodynamic field Figure (6) in the direction of the abscissa axis, scaled by the inlet velocity value, is shown on Figure 43.

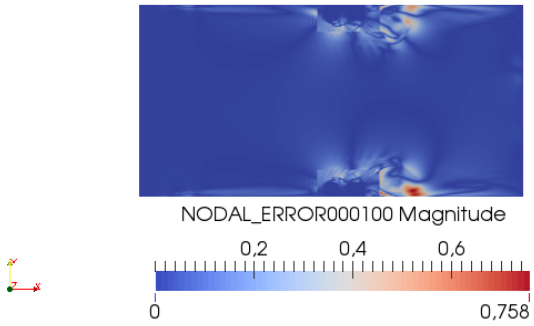

Figure 43: $\frac{|U_1(t,x,G^{New}) - U_1^{\mathrm{ROM}}(t,x,G^{New})|}{U_{inlet}}$

Furthermore, the relative X-global instantaneous error between the corrected flow field and the high fidelity one is plotted on Figure 44.

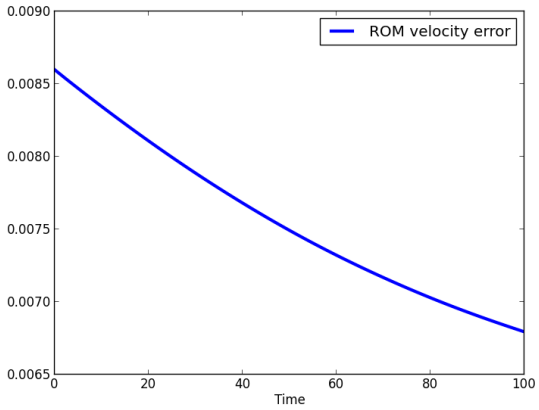

Figure 44: $\frac{\left\|U(t,G^{New})-U^{ROM}(t,G^{New})\right\|_X^2}{\|U(t,G^{New})\|_X^2}$

Conclusion and prospects

In this paper we have proposed a new method in order to tackle geometrical variabilities within the unsteady and incompressible Navier-Stokes equations. Our new algorithm is based on a hybrid approach in order to compute local LES around a new design definition and an adaptation of the classical Gappy-POD approach in order to tackle geometrical variations of turbulent fluid flows that might introduce irregularities in the flow topology and for which the classical Gappy-POD is no longer sufficient. The main idea is to update the reference POD basis of the Gappy-POD method by the coherent structures of the local LES of the new design. The optimization problem of the Gappy-POD is replaced in our method by a Galerkin projection of the governing Navier-Stokes equations on global and local POD modes with the new design. This new approach proved good results when applied to a typical aeronautical injection system. The speed-up associated with this technique is equal to 100, by taking into account the hybrid computation of the local LES in the RFD.

Acknowledgements

The authors of the paper would like to thank Vincent Moureau for his technical assistance with Yales2 and fruitful discussions.

References

N. Akkari, R. Mercier, G. Lartigue, V. Moureau, Stable pod-galerkin reduced order models for unsteady turbulent incompressible flows, 55th AIAA Aerospace Sciences Meeting, AIAA Science and Technology Forum and Exposition. Grapevine, Texas, USA (2017).

N. Akkari, F. Casenave, V. Moureau, Time stable reduced order modeling by an enhanced reduced order basis of the turbulent and incompressible 3d navierâĂŞstokes equations, Mathematical and Computational Applications 24 (2019).

R. Everson, L. Sirovich, Karhunen loeve procedure for gappy data, J. Opt. Soc. Am. A 8 (1995) 1657–1664.

T.Bui-Thanh, M. Damodaran, K. Willcox, Aerodynamic data reconstruction and inverse design using proper orthogonal decomposition, AIAA Journal 42 (2004).

N. E. Murray, J. M. Seiner, The effects of gappy pod on higher-order turbulence quantities, 46th AIAA Aerospace Sciences Meeting and Exhibit, Reno, Nevada (2008).

X. Csi, F. Ladeinde, A comparison of two pod methods for airfoil design optimization, 35th AIAA Fluid Dynamics conference and Exhibit, Toronto, Ontario, Canada (2005).

S. G. Raben, J. J. Charonko, P. P. Vlachos, Adaptive gappy pod for particle image velocimetry data reconstruction, Measurment Science and Technology 23 (2012).

Y. Duan, J. Cai, Y. Li, Gappy pod-based two step optimization for airfoil design, AIAA Journal 50 (2012).

M. Mifsud, A. Vendl, L.-U. Hansen, S. GÃűrtz, Fusing wind-tunnel measurements and cfd data using constrained gappy proper orthogonal decomposition, Aerospace Science and Technology 86 (2019) 312 – 326.

C. Jiang, Y. C. Soh, H. Li, Sensor and cfd data fusion for airflow field estimation, Applied Thermal Engineering 92 (2016) 149 – 161.

A. Hay, J. Borggaard, I. Akhtar, D. Pelletier, Reduced-order models for parameter dependent geometries based on shape sensitivity analysis, Journal of Computational Physics 229 (2010) 1327–1352.

B. A. Freno, P. G. Cizmas, A proper orthogonal decomposition method for nonlinear flows with deforming meshes, International Journal of Heat and Fluid Flow 50 (2014) 145 – 159.

L. Sirovich, Turbulence and the dynamics of coherent structures, Part III: dynamics and scaling. Quarterly of applied mathematics 45 (1987) 583–590.

N. Akkari, R. Mercier, V. Moureau, Geometrical reduced order modeling (rom) by proper orthogonal decomposition (pod) for the incompressible navier stokes equations, 2018 AIAA Aerospace Sciences Meeting, AIAA SciTech Forum, (AIAA 2018-1827) (2018).

V. Moureau, P. Domingo, L. Vervisch, Design of a massively parallel CFD code for complex geometries, Comptes Rendus Mécanique 339 (2011a) 141 – 148.

V. Moureau, P. Domingo, L. Vervisch, From large-eddy simulation to direct numerical simulation of a lean premixed swirl flame: Filtered laminar flame-PDF modeling, Combustion and Flame 158 (2011b) 1340 – 1357.

M. Malandain, N. Maheu, V. Moureau, Optimization of the deflated conjugate gradient algorithm for the solving of elliptic equations on massively parallel machines, Journal of Computational Physics 238 (2013).

W. Meier, P. Weigand, X. R. Duan, R. Giezendanner-Thoben, Detailed characterization of the dynamics of thermoacoustic pulsations in a lean premixed swirl flame, Combustion and Flame 150 (2007) 2–26.

P. Weigand, X. R. Duan, W. Meier, U. Meier, M. Aigner, C. Bérat, Experimental investigations of an oscillating lean premixed ch4-air swirl flame in a gas turbine model combustor, in: Proc. of the European Combustion Meeting 2005, 2005, p. 235.

G. Lartigue, U. Meier, C. Berat, Experimental and numerical investigation of self-excited combustion oscillations in a scaled gas turbine combustor, Applied thermal engineering 24 (2004) 1583–1592.

S. Roux, G. Lartigue, T. Poinsot, U. Meier, C. Bérat, Studies of mean and unsteady flow in a swirled combustor using experiments, acoustic analysis, and large eddy simulations, Combustion and Flame 141 (2005) 40–54.

V. Moureau, P. Minot, H. Pitsch, C. Bérat, A ghost-fluid method for large-eddy simulations of premixed combustion in complex geometries, Journal of Computational Physics 221 (2007) 600–614.

B. Fiorina, R. Vicquelin, P. Auzillon, N. Darabiha, O. Gicquel, D. Veynante, A filtered tabulated chemistry model for LES of premixed combustion, Combustion and Flame 157 (2010) 465–475.

B. Franzelli, E. Riber, L. Y. M. Gicquel, T. Poinsot, Large Eddy Simulation of combustion instabilities in a lean partially premixed swirled flame, Combustion and Flame 159 (2012) 621–637.

J. M. Lourier, M. Stöhr, B. Noll, S. Werner, A. Fiolitakis, Scale Adaptive Simulation of a thermoacoustic instability in a partially premixed lean swirl combustor, Combustion and Flame 183 (2017) 343–357.